NJC

PAPER

View Article Online
View Journal

Cite this: DOI: 10.1039/c8nj05375h

2-Methyl-substituted monotetrazoles in copper(II) perchlorate complexes: manipulating coordination chemistry and derived energetic properties†‡

Lukas Zeisel, Norbert Szimhardt, Maximilian H. H. Wurzenberger, Thomas M. Klapötke and Jörg Stierstorfer *

Received 23rd October 2018,
Accepted 26th November 2018

DOI: 10.1039/c8nj05375h

rsc.li/njc

A proposed correlation between coordination chemistry and deduced energetic properties (thermal behaviour, and sensitivities towards mechanical and optical stimuli) of copper(II) complexes is investigated. Starting from a system comprising $Cu(ClO_4)_2$ and either of the ligands 2-methyl-5-aminotetrazole (**1**, 2-MAT) or 2-methyl-5*H*-tetrazole (**2**, 2-MTZ), typically altered parameters like the metal(II) centre, ligand, or counterion were predefined. Instead, solely slight changes in ligand concentration and the solvent system were implemented in order to provide an insight into structure–property relationships of energetic coordination compounds (ECC) of this type. As a result, five highly energetic complexes $[Cu(H_2O)_2(2\text{-MAT})_4](ClO_4)_2\cdot H_2O$ (**3**), $[Cu(H_2O)_2(2\text{-MAT})_4](ClO_4)_2$ (**4**), $[Cu(H_2O)_2(2\text{-MAT})_4](ClO_4)_2\cdot 2$ 2-MAT (**5**), $[Cu(ClO_4)_2(H_2O)_2(2\text{-MAT})_2]$ (**6**), and $[Cu(H_2O)_2(2\text{-MTZ})_4](ClO_4)_2$ (**7**) were synthesized and, except for **5**, elaborately characterized. Besides structural elucidation *via* X-ray diffraction, NIR-spectroscopy, differential thermal analysis (DTA), standard sensitivity measurements (impact, friction, and electrostatic discharge), UV/vis-spectroscopy, and optical initiation experiments were conducted to deduce a precise relationship between coordination chemistry and the consequential energetic characteristics of these complexes.

Introduction

Dominated by the oxidation states +I and +II, copper exhibits diverse coordination chemistry. Especially the d^9 Cu^{II} cation is commonly applied in many areas of chemistry as the metal center of coloring agents,[1] insecticides,[2,3] catalysts,[4] and metalloproteins.[5] In most of these cases, copper(II)'s coordination chemistry is influenced by oxygen- and nitrogen-donating ligands, typically forming square planar, tetrahedral and, predominantly, octahedral coordination environments.[3]

In recent years, the growing field of energetic coordination compounds (ECC) has greatly benefited from promising Cu^{II} complexes. Due to the urgent necessity of substituting commonly applied, toxic primary explosives like lead azide and lead styphnate, an approach using significantly less toxic transition metal complexes appeared to be highly encouraging.[6]

In recent years, seminal reports from Shreeve,[7] Myers,[8] and Klapötke[9] set the stage for future applications of ECC. In targeting novel transition metal complexes with auspicious properties (convenient accessibility, thermal stability, and safe initiation), a consistently implemented general approach has emerged: starting from a desired transition metal cation with the corresponding counter-anion, energetic ligands, as well as the applied reaction conditions, offer precise tailoring of the desired characteristics.[7–9] Whereas variation of parameters like the ligand, metal centre, and anion tend to distinctly influence the coordination chemistry and the complexes' properties, additional fine tuning towards desired attributes might be achieved by accurately controlling the applied reaction conditions. While initial experiments in this direction have already led to sought results, a comprehensive report is still anticipated until today.[9b–12]

In regard to previously applied ligand systems, mostly nitrogen-rich, endothermic heterocycles were considered.[7–16] Among others, mono-substituted tetrazoles like the highly energetic 1,5-diaminotetrazole (1,5-DAT), 1-amino-5*H*-tetrazole (1-AT) and 2-amino-5*H*-tetrazole (2-AT) as well as 1-methyl-5*H*-tetrazole (1-MTZ) and 1-methyl-5-aminotetrazole (1-MAT) were investigated as ligands in ECC (Chart 1).[10,13,14] Hereby, the obtained transition metal complexes proved to be highly energetic, readily

Department of Chemistry, Ludwig Maximilian University Munich, Butenandtstrasse 5–13, Haus D, D-81377 Munich, Germany. E-mail: jstch@cup.uni-muenchen.de

† Dedicated to Prof. Dr Ingo-Peter Lorenz on the occasion of his 75th birthday.

‡ Electronic supplementary information (ESI) available: Experimental and general methods, X-ray diffraction, IR spectroscopy, DTA plots, TGA plots of **1**–**4**, hot plate and hot needle tests, and laser ignition tests. CCDC 1850124 (**3**), 1850121 (**4**), 1850122 (**5**), 1850120 (**6**) 1850123 (**7**). For ESI and crystallographic data in CIF or other electronic format see DOI: 10.1039/c8nj05375h

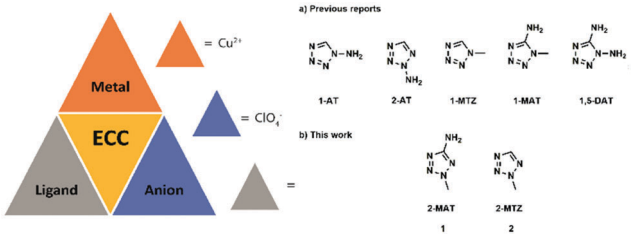

Chart 1 Precedents and current work using energetic monotetrazoles in ECC.

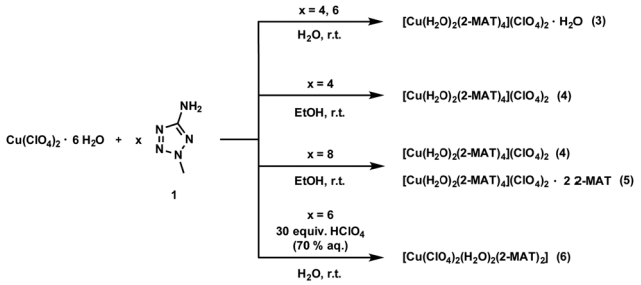

Scheme 1 Synthesis of complexes **3–6** using 2-methyl-5-aminotetrazole (**1**).

synthesized and partially exhibited auspicious properties as laser-ignitable primary explosives.[10,13]

Based on these results, the present work aims for a deeper insight into the possibility of precisely manipulating an ECC's coordination chemistry and the resulting energetic properties (sensitivities, thermal properties, and laser initiation) by solely modifying the reaction conditions (ligand concentration, solvent, and additives) in hand. Predefinitions for the applied systems included copper(II) as metal species, perchlorate counter-anions and, as an extension to previously published reports, 2-methyl-5-aminotetrazole (**1**, 2-MAT, $\Delta_f H^0_{(g)}$ = 2802 kJ kg^{-1})[17] and 2-methyl-5*H*-tetrazole (**2**, 2-MTZ, $\Delta_f H^0_{(g)}$ (2-MTZ) = 3347 kJ kg^{-1})[17] as endothermic ligands. Both nitrogen-rich heterocycles are expected to allow comparison to the respective 1-substituted tetrazoles and their energetic metal complexes. While recently published results from Szimhardt *et al.* provide a comprehensive study of 1-MTZ and its transition metal complexes,[10] only a few examples of 1-MAT ECC have been reported alongside a range of corresponding tetrazolium salts.[18–20] Moreover, and in relation to related, tremendously sensitive 2-aminotetrazole complexes,[13] 2-MAT and 2-MTZ incorporating ECC are proposed to combine efficient optical initiation with enhanced stability towards mechanical stimuli, thus allowing safe handling of these materials.

Results and discussion

Synthesis

Initially, nitrogen-rich ligand **1** was synthesized *via* a convenient, single step reaction using commercially available 5-aminotetrazole as a starting material (see Scheme S1, ESI‡). Due to the tautomerization of 1,5*H*-tetrazole, the dimethylsulfate-mediated methylation step provided the desired ligand alongside 1-methyl-5-aminotetrazole in a ratio of 3 : 4. With the targeted 2-MAT in hand, initial investigations concerning its coordination chemistry were accessed (Scheme 1).

The performed reactions were carried out at ambient temperature by slowly adding pre-dissolved ligand to a solution of copper(II) perchlorate. By solely applying a minimal amount of solvent, the crystallization process at room temperature could be accelerated. Thereby received solids were filtered off, washed with cold ethanol and dried in air, not requiring further purification.

As a starting point, 6 and 4 equivalents of 2-MAT were applied to an aqueous solution of $Cu(ClO_4)_2$ aiming for a frequently observed hexacoordinate copper(II) center.[10,21] In contrast to that and regardless of the applied ligand concentration, the present reaction provided $[Cu(H_2O)_2(2\text{-MAT})_4](ClO_4)_2{\cdot}H_2O$ (**3**) in 52% yield after four days of crystallization. Proceeding from these preliminary results, the utilization of a solvent with decreased polarity was tested. Using ethanol as the reaction medium and 4 equiv. of the ligand indeed led to the isolation of a new complex **4**. Nevertheless and despite successfully preventing the incorporation of cocrystallized water, $[Cu(H_2O)_2(2\text{-MAT})_4](ClO_4)_2$ (**4**) simultaneously retained the actual coordination sphere with two coordinating aqua ligands. To further extend this condition screening, an increased 2-MAT concentration (8 equivalents) was introduced while maintaining ethanol as the solvent. As a result and immediately after combining the ligand and copper(II) perchlorate, a light green precipitate occurred. After filtration, preliminary characterization of the residue by IR spectroscopy confirmed the formation of a previously unknown complex $[Cu(H_2O)_2(2\text{-MAT})_4](ClO_4)_2{\cdot}2$ 2-MAT (**5**) alongside ECC **4**. Since conducted attempts of clean isolation or purification of **5** proved to be unsuccessful, further characterization was impeded. Interestingly, the earlier collected filtrate of the present reaction once again provided **4** after crystallization for six days. A final attempt of interfering with the previously observed coordination chemistry of this system was to apply concentrated perchloric acid. According to reported syntheses, this approach promised a water-free ECC with enhanced energetic characteristics by substituting aqua ligands with coordinating perchlorate counter-anions.[22] Unfortunately, charging the aqueous reaction mixture with 30 equivalents of $HClO_4$ led to complex **6**, which still exhibited coordinating aqua ligands (yield: 76%). In contrast to previously obtained ECC, the coordination sphere of $[Cu(ClO_4)_2(H_2O)_2(2\text{-MAT})_2]$ indeed comprises two copper(II) associated perchlorato anions while solely exhibiting two equivalents of the nitrogen-rich ligand **1**. A possible and reoccurring explanation for a decrease of coordinating tetrazole ligands might be the protonation and simultaneous elimination of an N-coordination site.[9f,12] In comparison to that, the corresponding 1-methyl-5-aminotetrazole exhibited low solubility in water, thus leading to the reoccurring precipitation of the ligand.[19] Moreover, and whenever ligand crystallization could be prevented, collected X-ray data of isolated crystals repeatedly proved the simultaneous presence of multiple ECC species.[19]

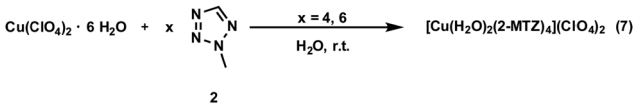

Scheme 2 Formation of the copper(II) perchlorate complex **7**.

Conclusively, 2-methyl-5*H*-tetrazole (2-MTZ) was investigated as a comparative example for additional 2-substituted monotetrazoles (Scheme 2). The ligand itself was accessed *via* a straightforward two-step reaction starting from basic building blocks (see Scheme S2, ESI‡). Once again, tautomerization led to a significant decrease in the yield of 2-MTZ due to the formation of isomeric 1-methyl-5*H*-tetrazole (1-MTZ) (1-MTZ/2-MTZ = 2 : 1).

When being applied to an aqueous solution of copper(II) perchlorate, 2-MTZ exhibits remarkable similarity to the previously investigated 2-MAT. In comparison to complexes **3** and **4**, $[Cu(H_2O)_2(2\text{-MTZ})_4](ClO_4)_2$ (**7**), which was isolated from the mother liquor after one day (yield: 73%), features almost equivalent coordination chemistry under identical reaction conditions. Moreover, and in contrast to the 2-MAT system, a change of solvent (ethanol) or stoichiometry (x = 4, 6, and 10) exclusively led to the same product **7**. Whenever the metal(II) center was altered (Fe^{2+}, Zn^{2+}, and Mn^{2+}) no crystallization of a potential ECC was achieved. Interestingly, and in accordance with previous reports, 2-substituted tetrazoles as ligands appear to consistently promote the incorporation of aqua ligands.[18b,21] Reasons for this could be the steric hindrance of six tetrazoles coordinating to the transition metal or the thermodynamically and kinetically preferred formation of more inert complexes. However, further studies including thermodynamic calculations are needed for the future.

Crystal structures

Since each of the obtained complexes was obtained as single crystals, structural characterization was conducted using low temperature X-ray diffraction. Measurement and refinement data are provided in the ESI.‡ Additionally, details of the obtained crystal structures were deposited in the CSD database and can be obtained free of charge from the CCDC: 1850124 (**3**), 1850121 (**4**), 1850122 (**5**), 1850120 (**6**), and 1850123 (**7**).‡[23] In terms of the observed coordination geometry, the examined copper(II) centres provided Jahn–Teller distorted octahedra, which consistently exhibited N4-coordinating ligands. Considering calculated electrostatic potentials at the respective ligand's binding sites (Fig. 1), the highest electron density of both 2-MAT and 2-MTZ occurs at the tetrazole's carbon–adjacent nitrogen N4, thus explaining the observed coordination behaviour observed by X-ray diffraction and additionally conducted IR spectroscopy (see ESI,‡ Fig. S1).

Ahead of the comprehensive analysis of received crystal structures it should be stated that structural data of coordinating 2-MAT and 2-MTZ consistently resemble corresponding, literature-known X-ray data of the respective non-coordinating ligand or comparable ECC and are therefore not discussed any further.[24,25]

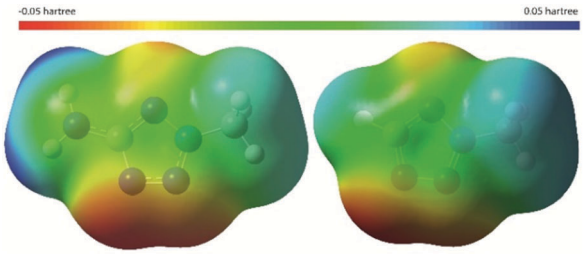

Fig. 1 Calculated (B3LYP/6-31G(d,p)) electrostatic potentials (3D isosurface of electron density) of 2-MAT (**1**, left) and 2-MTZ (**2**, right).

The first of the obtained complexes, $[Cu(H_2O)_2(2\text{-MAT})_4](ClO_4)_2{\cdot}H_2O$ (**3**), crystallizes in the form of blue blocks in the monoclinic space group $C2/c$ with 16 formula units per unit cell and a calculated density of 1.669 g cm^{-3} at 173 K. The Jahn–Teller distorted, octahedral copper(II) coordination sphere comprises two axial aqua and four equatorial 2-MAT ligands (Fig. 2) forming a slightly tilted O–Cu–O axis and a marginally distorted plane, respectively.

In addition to these observations in regard to the structure of a single complex unit, the three-dimensional topology of this compound reveals interesting stacking patterns (Fig. 3).

When viewing along the crystallographic b-axis, a chain pattern with alternating components can be observed. In addition to this ABAB pattern, whose ECC-layers are aligned along the crystallographic c-axis, equally oriented planes of perchlorate anions and cocrystallized water function as H-bond-mediating linkers between adjacent complex layers (Table 1). The aggregation of complexes to said layers equally benefits from intermolecular hydrogen bonding. In addition to that, viewing along the c-axis reveals a similar, but even more complex picture. While exhibiting the same ABAB pattern in between distinguishable chains, B lines further reveal an intrinsic CDCD motif along b.

Crystals of **4** have been isolated in the form of blue blocks in the monoclinic space group $P2_1$ with two formula units per unit

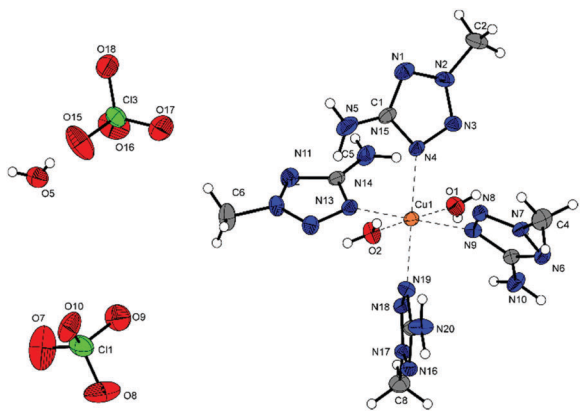

Fig. 2 Molecular unit of complex **3**. Thermal ellipsoids of non-hydrogen atoms in all structures are set to the 50% probability level. Selected bond lengths (Å): O1–Cu1 2.430(6), O2–Cu1 2.363(5), Cu1–N14 2.014(5), Cu1–N19 2.004(4), Cu1–N4 2.003(4), and Cu1–N9 2.008(5); selected bond angles (°): O1–Cu1–O2 177.2(2), N4–Cu1–O1 86.95(19), N4–Cu1–O2 93.91(18), N4–Cu1–N9 91.07(19), N4–Cu1–N14 88.89(19), N14–Cu1–O1 92.9(2), and N9–Cu1–O1 87.2(2).

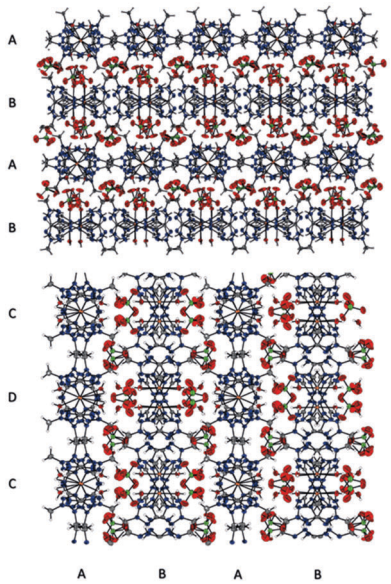

Fig. 3 Structure of **3** with the direction of view along the crystallographic *b*- (top) and *c*-axis (bottom).

Table 1 Lengths and angles of selected hydrogen bonds in **3**

D–H···A	*d*(D–H) [Å]	*d*(H···A) [Å]	*d*(D···A) [Å]	∠D–H···A [°]
N5–H5···N16	0.88	2.27	3.03	144.0
O3–H31···O6	0.83	1.89	2.71	173.6
N15–H15B···O9	0.88	2.57	2.96	107.0
N10–H10A···O9	0.88	2.17	3.02	163.0

cell and a calculated density of 1.788 g cm^{-3} at 173 K. The molecular unit consists of four 2-MAT and two aqua ligands once again resulting in an octahedral coordination sphere (Fig. 4). The corresponding perchlorate anions are non-coordinating. Regarding the appearance of the coordination polyhedron it becomes obvious that there is yet again a Jahn–Teller distortion to be observed along an axis that connects the copper(II) center with the two aqua ligands in axial positions. Considering these first observations it becomes clear that the structural parameters of **4** are almost identical to those of the previously discussed compound **3** with four 2-MAT ligands in the plane. The only significant differences such as the space group and the cell volume are caused by the absence of crystal water molecules. Another slight alteration can be observed regarding the bond angles between the coordinating ligands and copper(II), especially among the aqua and 2-MAT ligands. In the case of **4**, the bond angles approach the 90° of an ideal octahedron.

Crystallizing in the space group $P\bar{1}$, ECC **5** comprises two formula units per unit cell and has a calculated density of 1.699 g cm^{-3} at 173 K. The observed octahedral coordination sphere makes up the molecular unit including four 2-MAT and two aqua ligands. In addition, two equivalents of ligand **1** have been found as cocrystallized species (Fig. 5). Due to the reoccurring Jahn–Teller effect, the bond lengths along the tilted distortion axis O1–Cu1–O2 are significantly longer than those of the metal and the equatorial ligands. Since the equatorial 2-MAT-organized plane is not situated perpendicular on the O1–Cu1 and O2–Cu1 axes, a noticeable deviation from ideal flatness is observed.

As the final representative of the 2-MAT derived complexes, **6** crystallizes in the form of blue rods in the monoclinic space group $P2_1/n$ with two formula units per unit cell and a remarkably high calculated density of 1.997 g cm^{-3} at 173 K. Two asymmetric unit cells make up the molecular unit. The latter consists of a copper(II) center, and two aqua, two perchlorato, and two 2-MAT ligands forming a Jahn–Teller distorted, octahedral coordination sphere (Fig. 6).

The resulting polyhedron is made up of three straight axes which are caused by the fact that the two ligands of each kind coordinate *trans* to one another. The remaining four ligands are

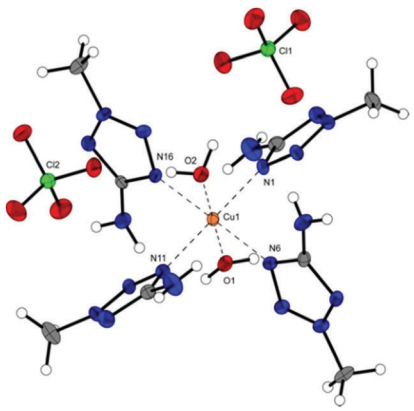

Fig. 4 Molecular unit of $[Cu(H_2O)_2(2\text{-MAT})_4](ClO_4)_2$ (**4**). Selected bond lengths (Å): O1–Cu1 2.417(5), O2–Cu1 2.397(5), N1–Cu1 1.999(5), N6–Cu1 2.049(6), N11–Cu1 2.000(5), and N16–Cu1 2.065(6); selected bond angles (°): O1–Cu1–O2 179.34(19), N1–Cu1–O1 87.6(2), N1–Cu1–O2 91.9(2), N6–Cu1–O1 88.2(2), N6–Cu1–O2 92.2(2), N16–Cu1–O1 90.85(19), and N16–Cu1–O2 88.8(2).

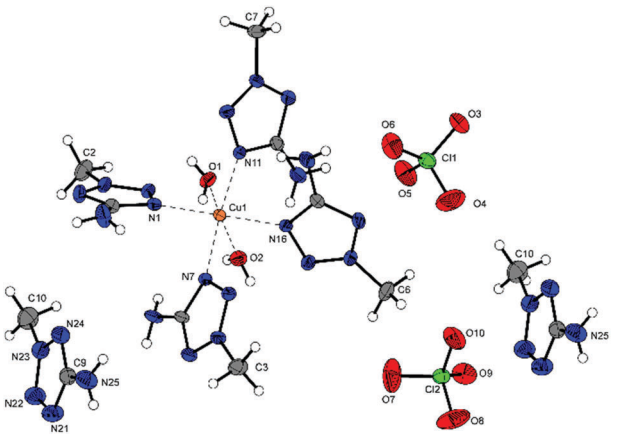

Fig. 5 Molecular unit of $[Cu(H_2O)_2(2\text{-MAT})_4](ClO_4)_2{\cdot}2$ 2-MAT (**5**). Selected bond lengths (Å): O1–Cu1 2.385(2), O2–Cu1 2.501(2), N1–Cu1 2.006(2), N7–Cu1 2.004(2), N11–Cu1 2.020(2), and N16–Cu1 2.000(2); selected bond angles (°): O1–Cu1–O2 173.44(7), N1–Cu1–O1 93.38(8), N1–Cu1–O2 92.11(8), N7–Cu1–O2 85.43(8), N16–Cu1–O2 85.14(8), N7–Cu1–N16 88.68(9), N11–Cu1–N16 86.82(9), N1–Cu1–N16 176.71(9), and N7–Cu1–N11 175.13(9); symmetry codes: (i) 1 − *x*, 1 − *y*, 1 − *z*, and (ii) −*x*, 2 − *y*, 1 − *z*.

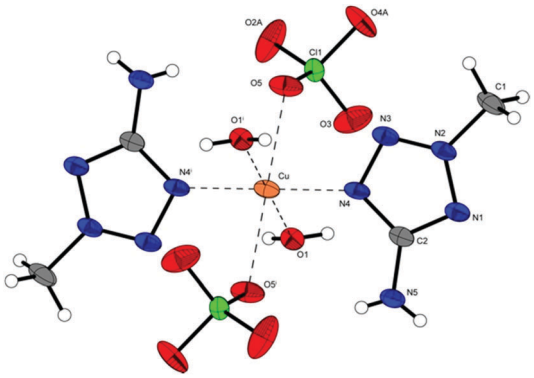

Fig. 6 Molecular unit of $[Cu(ClO_4)_2(H_2O)_2(2\text{-MAT})_2]$ (**6**). Selected bond lengths (Å): Cu1–O5 2.443(3), Cu1–N4 1.998(3), and Cu1–O1 1.960(3); selected bond angles (°): O1–Cu1–O5 96.32(10), O1–Cu1–O5^{i} 83.69(10), O1–Cu1–N4 90.59(12), O1–Cu1–N4^{i} 89.41(12), and O5–Cu1–O5^{i} 180.00; symmetry code: (i) 2 − *x*, −*y*, −*z*.

located in an ideal plane with bond lengths between the metal(II) center and the respective ligand being expectedly shorter than along the O5–Cu1–O5^{i} axis. Another significant deviation from an ideal octahedron can be observed regarding the bond angles between axial ligands and coordinating molecules in the equatorial plane. Lastly, the molecular structure of **7** was investigated. In analogy to complex **6**, $[Cu(H_2O)_2(2\text{-MTZ})_4](ClO_4)_2$ crystallizes in the monoclinic space group $P2_1/n$ (Z = 2), while exhibiting a significantly lower calculated density at 173 K (1.702 g cm^{-3}). As stated beforehand, the obtained crystal structure displays a remarkable resemblance to the molecular structures of **3** and **4** (Fig. 7). Nevertheless, copper(II)–aqua distances along the Jahn–Teller distorted O1–Cu–O1^{i} axis proved to be distinguishably shorter. Despite this deviation, measured torsion angles consistently exhibit values close to those of an ideal octahedron.

Thermal properties and sensitivities

Following the structural characterization of the received complexes, energetic properties in terms of thermal stability and sensitivities towards mechanical stimuli were investigated.

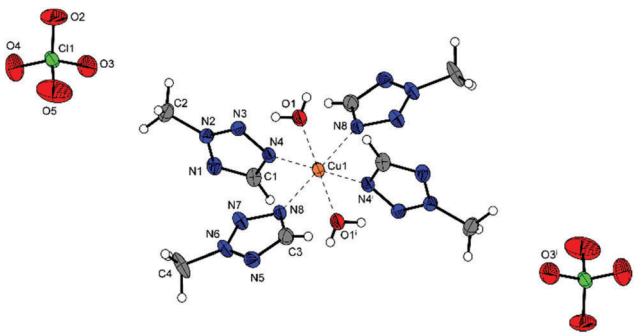

Fig. 7 Molecular unit of $[Cu(H_2O)_2(2\text{-MTZ})_4](ClO_4)_2$ (**7**). Selected bond lengths (Å): Cu1–O1 2.300(3), Cu1–N4 2.023(2), and Cu1–N8 2.029(2); selected bond angles (°): O1–Cu1–N4 93.15(11), O1–Cu1–N8 88.31(11), O1–Cu1–O1^{i} 180.00, N4–Cu1–N8 88.11(9), O1^{i}–Cu1–N8 91.69(11), and N4–Cu1–N4^{i} 180.00; symmetry code: (i) 1 − *x*, −*y*, 2 − *z*.

Thereby conducted differential thermal analysis (DTA, heating rate: β = 5 °C min^{-1}, see Table 2, Fig. S5, ESI‡) provided a distinct differentiation between uncoordinated ligands **1** and **2** and the obtained ECC. While the nitrogen-rich ligands 2-MAT (**1**) and 2-MTZ (**2**) both exhibit high thermal stability in the measured range of 25–400 °C, the corresponding copper(II) complexes each show exothermic decomposition temperatures from 171 °C (**4**) to 240 °C (**7**). Endothermic events observed for both ligands are assumed to be caused either by melting (T_{endo1} (**1**)) or evaporation of the compound (T_{endo2} (**1**), T_{endo1} (**2**), see corresponding TGA plots, Fig. S6, ESI‡). Whereas the loss of cocrystallized water in the DTA measurement of **4** solely marginally influences the determined exothermic decomposition temperature, it seems possible that in **3** a slow decomposition starts before the onset temperature of 176 °C. In the case of the structurally analogous complexes **3**, **4**, and **7**, endothermic events which are most likely caused by evaporation of cocrystallized or coordinated water were detected in an expectedly narrow range (125 °C (**3**), 110 °C (**4**), and 115 °C (**7**)). To gain a better understanding of this partial ECC decomposition prior to the actual exothermic event, thermal gravimetric analysis was implemented for ECC **3**, **4** (see ESI,‡ Fig. S6), and $[Cu(H_2O)_2(2\text{-MTZ})_4](ClO_4)_2$ (**7**) (Fig. 8).

Whereas TGA plots of **3** and **4** (see ESI,‡ Fig. S6) show an almost continuous loss of the compounds' mass between 100 and 250 °C and no sharp mass decrease at the decomposition temperature, the corresponding plot of **7** exhibits distinct disintegration events. Affirmatively, the observed mass loss starting below 100 °C (5.67%) can be assigned to the loss of present aqua ligands and refers to the first endothermic event (115 °C) during the DTA measurement. Moreover, T_{endo2} (DTA: 208 °C) was confirmed by a matching 26.5% mass loss during

Table 2 Thermal stability measurements of **1–4**, **6**, and **7** by DTA[a]

Compound	T_{endo1}[b] [°C]	T_{endo2}[b] [°C]	T_{exo}[c] [°C]
1	104	252	—
2	152	—	—
3	125	—	176
4	110	—	171
6	—	—	192
7	115	208	240

[a] Onset temperatures at a heating rate of β = 5 °C min^{-1}. [b] Endothermic peak, which indicates melting, dehydration, or loss of coordinating or cocrystallized molecules. [c] Exothermic peak, indicating decomposition.

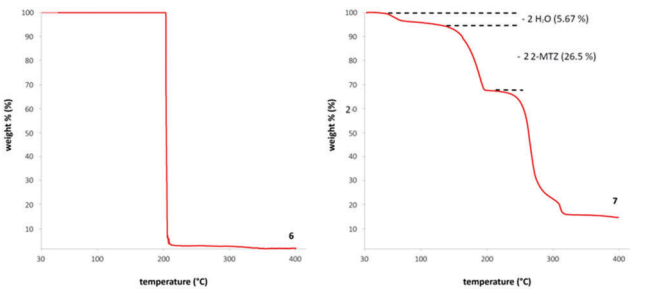

Fig. 8 TGA measurements (5 °C min^{-1}) of **6** and **7**.

the TGA measurement, a fact that presumably is effected by ligand evaporation. The final step of decomposition is identified by an exothermic event at the remarkably high temperature of 240 °C. Lastly, complex **6**, which exhibited two copper(II)–perchlorato bonds, proved to similarly disintegrate at high, but slightly lower temperatures without indicating an event of endothermic decomposition (Table 2 and Fig. 8). In order to explain this rather unusual observation, one might consult the complex's coordination chemistry: contrary to complexes **3**, **4**, **5**, and **7**, coordinating aqua ligands are in the plane and exhibit significantly shortened ($\approx$0.4 Å) copper–aqua bond lengths which presumably lead to aggravated dissociation. Additionally, the sharp mass loss observed during TGA measurements further proves ECC **6** remains in its distinct composition until being exposed to its decomposition temperature (Fig. 8). Resulting from the observed thermal properties, the incorporation of cocrystallized water and the introduction of coordinating perchlorato anions cause a measurable increase in thermal stability.[10,22]

Regarding the investigated compounds' sensitivities towards mechanical stimuli, **1** and **2** both can be classified as insensitive according to UN standards (impact: >40 J, friction: >360 N). In contrast to that, introducing the highly oxidizing perchlorate anion and a coordination site like copper(II) once more proves the potential of the ECC approach due to the formation of distinctly more sensitive compounds (Table 3). Considering the series of 2-MAT based copper(II) complexes, one might recognize the tendency that with decreasing content of water, more specifically the loss of the cocrystallized species, the resulting complexes show increased sensitivities (**3** *vs.* **4** and **6**).[10] Unfortunately, proceeding from this initial proposition, ECC **4**, **6**, and **7** each exhibit sensitivities at the lower end of the measuring range. As a result, a quantitative evaluation of sought structure–property relationships most likely is prevented by possibly varying fractal characteristics and particle sizes.[26] Moreover, the correlation between sensitivities and molecular structure is proposed to be dependent on multiple factors like oxygen balance (OB),[27] the electronic band gap,[28] molecular electrostatic potentials,[29] and dissociation energies of critical bonds.[30] Nevertheless, complex **6**, which exhibits the lowest nitrogen ("propellant") content and the OB closest to 0 represents the overall most sensitive compound in terms of impact and friction and can be compared to the analogous chlorate complex.[18b] ECC **4**, which, in comparison to structurally equivalent **7**, incorporates the less energetic ligand, displays a higher nitrogen content and exhibits the highest sensitivities towards impact and electrostatic discharge. Conducted hot plate and hot needle tests for each of the characterized ECC showed sharp deflagration events (see ESI,‡ Fig. S9–S14).

Table 3 Sensitivities towards the external stimuli impact, friction, and ESD

Compound	IS[a] [J]	FS[b] [N]	ESD[c] [mJ]	Grain size [μm]
1	>40	>360	1500	100–500
2	>40	>360	—	100–500
3	5	30	260	500–1000
4	<1	24	20	<100
6	2	2.2	150	<100
7	5	5	50	100–500

[a] Impact sensitivity according to the BAM drophammer (method 1 of 6). [b] Friction sensitivity according to the BAM friction tester (method 1 of 6). [c] Electrostatic discharge sensitivity (OZM ESD tester); impact: insensitive >40 J, less sensitive ≥35 J, sensitive ≥4 J, very sensitive ≤3 J; friction: insensitive >360 N, less sensitive = 360 N, sensitive <360 N and >80 N, very sensitive ≤80 N, extremely sensitive ≤10 N. According to the UN Recommendations on the Transport of Dangerous Goods.

Optical initiation and UV-vis spectroscopy

In addition to the well-established initiation of energetic compounds *via* mechanical and thermal stimuli, recent developments in this field dealt with the neglected sensitivities of these species towards optical initiation.[10,21,31] Until today, a broad range (Mn, Fe, Co, Ni, Cu, and Zn) of 3d transition metal complexes and energetic materials have been successfully initiated *via* laser irradiation while an unambiguous mechanistic proposal is still awaited. On one hand, common suggestions discuss a photochemical initiation mechanism through an excitation–relaxation process during which photonic energy is translated to the decomposition-initiating vibrational energy.[9c,32] Additionally, a reoccurring proposal deals with a photothermal mechanism, during which photonic energy is directly converted into lattice heat and vibrational energy, which according to the "hot-spot"-theory further leads to decomposition of the material.[10,32b] To investigate the optical sensitivities of **3**–**7** and a possible coherence with either of the proposed initiation mechanisms, laser initiation experiments were conducted along with UV-vis spectroscopy (Table 4 and Fig. 9). The distinction between deflagration and detonation was made by means of acoustic output and high-speed recordings (Fig. S7, ESI‡).

While each of the investigated ECC showed a reaction resulting from the applied conditions, solely perchlorato ligand incorporating complex **6**, as well as the 2-MTZ complex **7**, detonated in the course of the experiment.

While **3** exhibited sharp deflagration upon laser irradiation, **4** solely decomposed without any sign of an exothermic reaction. Resulting from that, an unambiguous confirmation of either of the proposed initiation mechanisms (photochemical or thermal) remains anticipated. In contrast to the literature, the comparably strong response of the least sensitive compound **3**

Table 4 Results of laser ignition tests[a] and UV-vis spectroscopy

Compound	Reaction	Color	λ_{d-d}[b]	$OD(\lambda_{915})/OD(\lambda_{d-d})$[c]
3	deflag.	Blue	613	0.39
4	dec.	Blue	620	0.37
6	det.	Blue	658	0.46
7	det.	Blue	681	0.34

[a] dec.: decomposition, deflag.: deflagration, det.: detonation. Operating parameters: current I = 7 A; voltage U = 4 V; theoretical maximal output power P_{max} = 45 W; theoretical energy E_{max} = 0.17 mJ; wavelength λ = 915 nm; pulse length τ = 0.1 ms. [b] Absorption intensity maximum wavelength, which can be assigned to electron d–d excitations in the measured range of 350–1000 nm. [c] Quotient of the absorption intensity at the laser wavelength and the intensity at the d–d absorption wavelength.

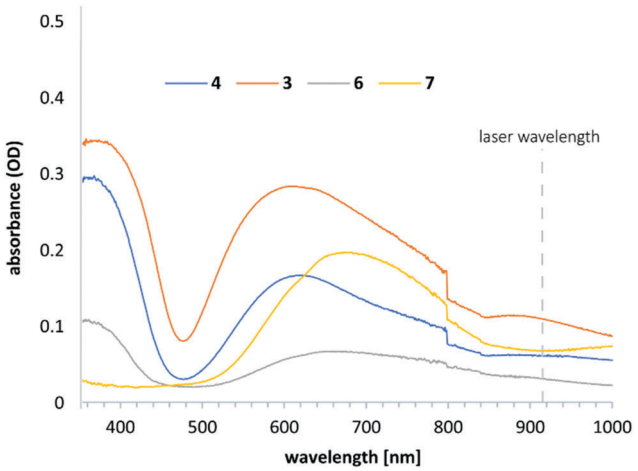

Fig. 9 Solid state UV/vis spectra of selected copper(II) and iron(II) complexes. The step in the absorption intensity at 800 nm is caused by a detector change. The UV-vis spectra have only qualitative character.

towards optical stimuli suggests no distinct correlation between mechanical and optical sensitivites, further being proved by the observed difference between **4** and **7**.[10,12,21] Furthermore, an obvious coherence between thermal properties (see Table 2) and optical initiation is equally prohibited since **6** and **7**, which proved to be highly thermally stable, gave the most violent responses upon laser irradiation (see ESI,‡ Fig. S7). Regarding the densities of the complexes and their outcome in the initiation tests, no general trend can be observed. Whereas compound **6** shows the highest density and a positive result in the experiments, complex **3** with the lowest one gives a stronger response to irradiation than compound **4**. Conducted solid state UV/vis measurements, which solely provide qualitative information, equally lack unequivocal trends (Fig. 9). To begin with, the spectra of **3** and **4**, both reacting noticably differently during laser experiments, are almost identical in terms of the observed d–d-transitions (613 and 620 nm) and curve shape. Moreover, the detected absorbance of the applied radiation (915 nm) solely corresponds to a fraction of the d–d-transition's maximum (see Table 4). Resulting from these conclusions, a desired correlation between coordination chemistry and optical sensitivity once again remained unfulfilled. Based on the previously noted, vague but highly relevant impact of fractal characteristics and the overall inconclusive current state of research in the field of laser-ignitable ECC, further investigations remain indispensable.

Conclusions

In summary, a series of energetic copper(II) perchlorate complexes were successfully synthesized and characterized by manipulating the present coordination chemistry through adjusting the parameters of the solvent, stoichiometry, acidity, and the applied 2-substituted tetrazole ligand. In regard to the 2-MAT complexes $[Cu(H_2O)_2(2\text{-}MAT)_4](ClO_4)_2{\cdot}H_2O$ (**3**), $[Cu(H_2O)_2(2\text{-}MAT)_4](ClO_4)_2$ (**4**) and $[Cu(ClO_4)_2(H_2O)_2(2\text{-}MAT)_2]$ (**6**), a decrease of the compound's water content as well as the incorporation of perchlorato ligands led to a rough increase of thermal stability and overall sensitivity. Inconsistencies, especially in regard to measured sensitivities and laser ignitability, might be attributed to fractal characteristics and particle sizes. Introducing a new nitrogen-rich ligand with increased energetic character (2-MTZ, **2**) results in novel patterns of the examined properties despite identical coordination chemistry (**7** *vs.* **4**). In the present case, higher thermal stability was accompanied by an increase in optical and friction sensitivity and a simultaneous decrease of ESD and impact sensitivities. Consequently, the present report provides lead-off insights into the correlation of an ECC's coordination chemistry and derived energetic properties, while future investigations might further develop observed patterns. Moreover, the obtained complexes, especially **6** and **7**, indeed meet targeted properties including exceptionally high thermal stability, decreased mechanical sensitivities in comparison to the 2-aminotetrazole ECC and retained laser ignitability. Therefore, both conveniently synthesized ECC represent promising candidates for being applied in future ignition (optical or mechanical) systems.

Conflicts of interest

There are no conflicts to declare.

Acknowledgements

Financial support of this work by the Ludwig Maximilian University of Munich (LMU) and the Office of Naval Research (ONR) under grant no. ONR.N00014-16-1-2062 is acknowledged. Furthermore, the authors want to thank Mr Michael Gruhne and Mr Marcus Lommel for their great help with the sensitivity determinations.

Notes and references

1 (*a*) E. Platania, N. L. W. Streeton, H. Kutzke, A. Karlsson, E. Uggerud and N. H. Andersen, *Vib. Spectrosc.*, 2018, **97**, 66–74; (*b*) S. Bette, R. K. Kremer, G. Eggert and R. E. Dinnebier, *Dalton Trans.*, 2018, **47**, 8209–8220.

2 (*a*) F. Brunel, N. E. El Gueddari and B. M. Moerschbacher, *Carbohydr. Polym.*, 2013, **92**, 1348–1356; (*b*) S. Chandraleka and G. Chandramohan, *Int. J. ChemTech Res.*, 2014, **6**, 5450–5457.

3 R. R. Conry, Copper: Inorganic & Coordination Chemistry, *Encyclopedia of Inorganic Chemistry*, John Wiley & Sons, Ltd., 1st edn, 2006.

4 (*a*) H.-J. Zhang, A. W. Schuppe, S.-T. Pan, J.-X. Chen, B.-R. Wang, T. R. Newhouse and L. Yin, *J. Am. Chem. Soc.*, 2018, **140**, 5300–5310; (*b*) S. B. Thorpe, J. A. Calderone and W. L. Santos, *Org. Lett.*, 2012, **14**, 1918–1921; (*c*) P. C. Roest, N. W. M. Michel and R. A. Batey, *J. Org. Chem.*, 2016, **81**, 6774–6778.

5 (*a*) P. L. Holland and W. B. Tolman, *Coord. Chem. Rev.*, 1999, **190–192**, 855–869; (*b*) W. L. Nettles, H. Song, E. R. Farquhar, N. C. Fitzkee and J. P. Emerson, *Inorg. Chem.*, 2015, **54**(12),

5671–5680; (*c*) C. A. Blasie and J. M. Berg, *J. Am. Chem. Soc.*, 2003, **125**, 6866–6867.
6 T. M. Klapötke, *Chemistry of High-Energy Materials*, Walter de Gruyter, Berlin, Boston, 2nd edn, 2012.
7 (*a*) G.-H. Tao, D. A. Parrish and J. M. Shreeve, *Inorg. Chem.*, 2012, **51**, 5305–5312; (*b*) R. P. Singh, R. D. Verma, D. T. Meshri and J. M. Shreeve, *Angew. Chem., Int. Ed.*, 2006, **45**, 3584–3601; (*c*) Q. Zhang and J. M. Shreeve, *Angew. Chem., Int. Ed.*, 2014, **53**, 2540–2542.
8 (*a*) T. W. Myers, D. E. Chavez, S. K. Hanson, R. J. Scharff, B. L. Scott, J. M. Veauthier and R. Wu, *Inorg. Chem.*, 2015, **54**, 8077–8086; (*b*) T. W. Myers, K. E. Brown, D. E. Chavez, R. J. Scharff and J. M. Veauthier, *Inorg. Chem.*, 2017, **56**, 2297–2303; (*c*) T. W. Myers, J. A. Bjorgaard, K. E. Brown, D. E. Chavez, S. K. Hanson, R. J. Scharff, S. Tretiak and J. M. Veauthier, *J. Am. Chem. Soc.*, 2016, **138**, 4685–4692.
9 (*a*) M. Friedrich, J. C. Gálvez-Ruiz, T. M. Klapötke, P. Mayer, B. Weber and J. J. Weigand, *Inorg. Chem.*, 2005, **44**, 8044–8052; (*b*) G. Geisberger, T. M. Klapötke and J. Stierstorfer, *Eur. J. Inorg. Chem.*, 2007, 4743–4750; (*c*) M. Joas, T. M. Klapötke, J. Stierstorfer and N. Szimhardt, *Chem. – Eur. J.*, 2013, **19**, 9995–10003; (*d*) M. Joas, T. M. Klapötke and N. Szimhardt, *Eur. J. Inorg. Chem.*, 2014, 493–498; (*e*) M. Joas and T. M. Klapötke, *Z. Anorg. Allg. Chem.*, 2014, **640**, 1886–1891; (*f*) T. M. Klapötke, P. C. Schmid, J. Stierstorfer and N. Szimhardt, *Z. Anorg. Allg. Chem.*, 2016, **642**, 383–389.
10 N. Szimhardt, M. H. H. Wurzenberger, A. Beringer, L. J. Daumann and J. Stierstorfer, *J. Mater. Chem. A*, 2017, **5**, 23753–23765.
11 J. Evers, I. Gospodinov, M. Joas, T. M. Klapötke and J. Stierstorfer, *Inorg. Chem.*, 2014, **53**, 11749–11756.
12 N. Szimhardt and J. Stierstorfer, *Chem. – Eur. J.*, 2018, **24**, 2687–2698.
13 N. Szimhardt, M. H. H. Wurzenberger, L. Zeisel, M. S. Gruhne, M. Lommel and J. Stierstorfer, *J. Mater. Chem. A*, 2018, **6**, 16257–16272.
14 (*a*) Y. Cui, T.-L. Zhang, J.-G. Zhang, L. Yang, X.-C. Hu and J. Zhang, *J. Mol. Struct.*, 2008, **889**, 177–185; (*b*) Y. Cui, J. Zhang, T. Zhang, L. Yang, J. Zhang and X. Hu, *J. Hazard. Mater.*, 2008, **160**, 45–50.
15 A. V. Smirnov, M. A. Ilyushin and I. V. Tselinskii, *Russ. J. Appl. Chem.*, 2004, **77**, 794–796.
16 Y. Xu, W. Liu, D. Li, H. Chen and M. Lu, *Dalton Trans.*, 2017, **46**, 11046–11052.
17 Gas phase enthalpies of formation were calculated using the atomization method ($\Delta_f H^0_{(g,M)} = H_{(M)} - \Sigma H^0_{(A)} + \Sigma \Delta_f H^0_{(A)}$) using Gaussian09 computed CBS-4M electronic enthalpies.
18 (*a*) A. Y. Zhilin, M. A. Ilyushin, I. V. Tselinskii, A. S. Kozlov and N. E. Kuz'mina, *Russ. J. Appl. Chem.*, 2002, **75**, 1849–1851; (*b*) M. H. H. Wurzenberger, N. Szimhardt and J. Stierstorfer, *J. Am. Chem. Soc.*, 2018, **140**, 3206–3209.
19 H. Radies, *Synthesis and Characterization of Energetic Transition Metal–Tetrazolate Complexes*, Diploma thesis, Ludwig Maximilian University of Munich, 2006.
20 (*a*) K. Karaghiosoff, T. M. Klapötke, P. Mayer, C. M. Sabaté, A. Penger and J. M. Welch, *Inorg. Chem.*, 2008, **47**, 1007–1019; (*b*) T. M. Klapötke and J. Stierstorfer, *Eur. J. Inorg. Chem.*, 2008, 4055–4062; (*c*) T. M. Klapötke and C. M. Sabaté, *Eur. J. Inorg. Chem.*, 2008, 5350–5366.
21 N. Szimhardt, M. H. H. Wurzenberger, T. M. Klapötke, J. T. Lechner, H. Reichherzer, C. C. Unger and J. Stierstorfer, *J. Mater. Chem. A*, 2018, **6**, 6565–6577.
22 M. Freis, T. M. Klapötke, J. Stierstorfer and N. Szimhardt, *Inorg. Chem.*, 2017, **56**, 7936–7947.
23 Crystallographic data for the structures have been deposited. with the Cambridge Crystallographic Data Centre.‡
24 J. H. Bryden, *Acta Crystallogr.*, 1956, **9**, 874–878.
25 (*a*) P. N. Gaponik, M. M. Degtyarik, A. S. Lyakhov, V. E. Matulis, O. A. Ivashkevich, M. Quesada and J. Reedijk, *Inorg. Chim. Acta*, 2005, **358**, 3949–3957; (*b*) E. J. van den Huevel, P. L. Franke, G. C. Verschoor and A. P. Zuur, *Acta Crystallogr.*, 1983, **39**, 337–339.
26 (*a*) X. Song, Y. Wang, C. An, X. Guo and F. Li, *J. Hazard. Mater.*, 2008, **159**, 222–229; (*b*) Y. Wang, X. Song, D. Song, W. Jiang, H. Liu and F. Li, *Propellants, Explos., Pyrotech.*, 2011, **36**, 505–512.
27 C. B. Storm, J. R. Stine and J. F. Kramer, *Chem. Phys. Energ. Mater.*, 1990, **309**, 605–639.
28 W. Zhu and H. Xiao, *Struct. Chem.*, 2010, **21**, 657–665.
29 P. Politzer and J. S. Murray, *J. Mol. Model.*, 2015, **21**, 25.
30 D. Mathieu, *Ind. Eng. Chem. Res.*, 2017, **56**, 8191–8201.
31 (*a*) M. T. Greenfield, S. D. McGrane, C. A. Bolme, J. A. Bjorgaard, T. R. Nelson, S. Tretiak and R. J. Scharff, *J. Phys. Chem. A*, 2015, **119**, 4846–4855; (*b*) A. E. Sifain, J. A. Bjorgaard, T. W. Myers, J. M. Veauthier, D. E. Chavez, O. V. Prezhdo, R. J. Scharff and S. Tretiak, *J. Phys. Chem. C*, 2016, **120**, 28762–28773; (*c*) E. D. Aluker, A. G. Krechetov, A. Y. Mitrofanov, D. R. Nurmukhametov and M. M. Kuklja, *J. Phys. Chem. C*, 2011, **115**, 6893–6901.
32 (*a*) D. D. Dlott and M. D. Fayer, *J. Chem. Phys.*, 1990, **92**, 3798–3812; (*b*) E. D. Aluker, A. S. Zverev, A. G. Krechetov, A. Yu. Mitrofanov, A. O. Terentyeva and A. V. Tupitsyn, *Russ. J. Phys. Chem. B*, 2014, **8**, 687–691.

